ACS ES&T Air

pubs.acs.org/estair

Article

Dependence of Reactive Oxygen Species Formation on the Oxidation State of Biogenic Secondary Organic Aerosols

Published as part of ACS ES&T Air special issue "John H. Seinfeld Festschrift".

Kasey C. Edwards, Lena Gerritz, Meredith Schervish, Manjula Canagaratna, Anita M. Avery, Mitchell W. Alton, Lisa M. Wingen, Jackson T. Ryan, Celia L. Faiola, Andrew T. Lambe, Sergey A. Nizkorodov, and Manabu Shiraiwa*

Cite This: *ACS EST Air* 2025, 2, 1738–1749

Read Online

ACCESS | Metrics & More | Article Recommendations | Supporting Information

ABSTRACT: Reactive oxygen species (ROS) play a central role in the chemical aging of organic aerosols and adverse aerosol health effects upon respiratory deposition. Previous research has shown that biogenic secondary organic aerosols (SOA) form ROS, including hydroxyl radicals and superoxide, via reactions of reactive compounds, including organic hydroperoxides and alcohols in the aqueous phase. However, the influence of oxidative aging and the SOA oxidation state on the ROS yield has not been systematically investigated. In this study, we quantify ROS yields in D-limonene SOA and β-caryophyllene SOA generated via $^{\bullet}$OH and $^{\bullet}$Cl oxidation in an oxidation flow reactor at equivalent atmospheric aging times ranging from 4 h to 22 days. We quantify radical formation using electron paramagnetic resonance spectroscopy combined with a spin-trapping technique and characterize the molecular composition of the SOA samples with high-resolution mass spectrometry. We observe maximum radical formation at an oxygen-to-carbon ratio (O/C) of ∼0.5. Thereafter, we observe a >90% decrease in radical yield as the O/C increases to 1.2 for both D-limonene SOA and β-caryophyllene SOA. Similarly, the radical yield in D-limonene and β-caryophyllene SOA is reduced by >80% after on-filter photoirradiation. Peroxide yields are found to decrease with increasing O/C values and irradiation, suggesting that the aging-induced fragmentation and/or photolysis of hydroperoxides contribute to a decrease of radical formation in aged SOA.

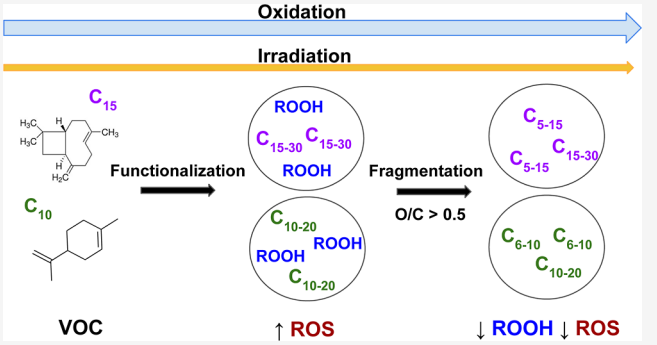

KEYWORDS: *oxidation, photooxidation, aging, reactive oxygen species, secondary organic aerosol*

1. INTRODUCTION

Emissions of biogenic volatile organic compounds (BVOCs), including monoterpenes ($C_{10}H_{16}$) and sesquiterpenes ($C_{15}H_{24}$), contribute around 1 Pg of carbon to the atmosphere annually.[1] Emissions of BVOCs are an order of magnitude larger than anthropogenic emissions, and oxidation of BVOCs contributes significantly to the formation of secondary organic aerosols (SOA).[2] Further multiphase oxidation leads to chemical transformation of SOAs, enhancing hygroscopic properties and cloud condensation nuclei (CCN) activity[3−5] and altering health-related properties.[6,7] Photolytic aging can alter the optical properties of SOA particles,[8] increase their viscosity,[9] and result in mass loss through fragmentation.[10,11] SOA compounds first undergo functionalization and then fragmentation as they are oxidized.[12−14] It has been shown that a semivolatile oxidized organic aerosol with an O/C of 0.35 ± 0.25[15,16] photochemically ages along a H/C vs O/C slope of ∼−0.5, resulting in low-volatility compounds.[15,16] Extremely low-volatility compounds (ELVOCs) and highly oxidized organic molecules (HOMs) with O/C greater than 0.7 can be formed via autoxidation, leading to peroxide functionality.[17,18] It was found that decomposition of peroxide-containing HOMs was associated with an increase in SOA oxidation state.[19]

Reactive oxygen species (ROS) play an important role in chemical aging of organic aerosols and adverse aerosol health effects.[20] Inhalation and respiratory deposition of aerosols can lead to the release of ROS, which can cause oxidative stress and onset of inflammatory response.[21] ROS include hydrogen peroxide (H_2O_2), superoxide ($O_2^{\bullet-}$), hydroxyl ($^{\bullet}$OH), and organic radicals.[20,22] Aqueous-phase decomposition of organic

Received: April 21, 2025
Revised: July 16, 2025
Accepted: July 17, 2025
Published: July 23, 2025

https://doi.org/10.1021/acsestair.5c00133
ACS EST Air 2025, 2, 1738–1749

hydroperoxides and HOMs can lead to the formation of •OH and organic radicals,[23,24] and subsequent reactions involving alcohols can result in the production of $O_2^{\bullet-}$, H_2O_2, and organic radicals.[22] Photoirradiation of SOA can also induce ROS formation via photolysis of hydroperoxides and carbonyls.[25,26] Organic peroxides are known to contribute substantially to SOA mass,[21,27] but with increased aging, peroxide content of SOA has been shown to both increase[28] and decrease.[29−33] One study found peroxide content and cell toxicity to increase with an aged naphthalene SOA.[28] In another study, a fresh or moderately aged SOA was found to have higher oxidative potential than a more aged SOA due to the decrease of peroxides and quinones.[34] In addition, H_2O_2 and H_2O_2 equivalent ROS (measured with the dichlorodihydrofluorescein assay) have been observed to decrease with aging in both laboratory and ambient samples,[35−37] while another study observed increase upon aging.[38] Direct measurement of the radicals and peroxides generated in aqueous solutions from SOA by varying the O/C has yet to be conducted and may provide insights into health implications of aged SOA.

In this study, we generated SOA samples from D-limonene and β-caryophyllene using an oxidation flow reactor (OFR) under varying oxidizing conditions to evaluate the effects of the SOA oxidation state on ROS formation. SOA samples were formed using either •OH or chlorine atoms (•Cl) as an oxidant. D-Limonene and β-caryophyllene were chosen as representative monoterpene and sesquiterpene, respectively: D-limonene is a major monoterpene species from biogenic emissions and a dominant constituent of volatile chemical products;[39,40] β-caryophyllene is a dominant sesquiterpene with high SOA yield.[1,41] We used online aerosol mass spectrometry to determine the average oxidation state (OS_C) and oxidation state (O/C) of SOA compounds. Electron paramagnetic resonance (EPR) spectroscopy was used to directly measure radicals from SOA in the aqueous phase.[42,43] High-resolution mass spectrometry was used offline to determine the chemical composition of SOA with varying oxidation states. Peroxide contents were quantified from SOA with different oxidants and photoaging times. The key observation of this work is a drastic reduction in ROS formation from SOA upon oxidative and photolytic aging.

2. METHODS

2.1. SOA Generation. We generated SOA particles via gas-phase •OH or •Cl oxidation of D-limonene or β-caryophyllene, followed by homogeneous nucleation in a Potential Aerosol Mass (PAM) Dual OFR (Aerodyne Research, Inc.) at Aerodyne Research.[44] The PAM Dual OFR consists of two horizontal 13 L aluminum cylindrical chambers (46 cm long × 22 cm ID) operating in continuous flow mode, with a 7.0−7.5 L min^{-1} flow through the reactor. One chamber was used for •Cl oxidation and the other for •OH oxidation. For SOA collection used in total peroxide measurements and irradiation experiments, we additionally generated SOA particles using an OFR deployed at UC Irvine with a 7.5 L min^{-1} flow through the reactor. The mean residence time in all OFRs, calculated by dividing the reactor volume by the total gas flow rate, ranged from 104 to 111 s. At Aerodyne Research, liquid solutions containing D-limonene, β-caryophyllene, or β-caryophyllene diluted to 10% (v/v) in carbon tetrachloride were injected into the OFR carrier gas at liquid flow rates ranging from 1 to 5 μL h^{-1} using a syringe pump. At UC Irvine, liquid D-limonene or β-caryophyllene was placed in an open vial inside a sealed glass container and evaporated into a 100−500 cm^3 min^{-1} carrier gas flow.

In the OFR used for •Cl oxidation, a compressed gas cylinder with 0.1% Cl_2 was diluted to approximately 10−15 ppmv Cl_2, which was then photolyzed at λ = 369 nm to form •Cl.[44] For the •OH OFR, the radicals were generated from the combined photolysis of O_2 and H_2O at λ = 185 nm plus photolysis of O_3 at λ = 254 nm, with secondary chemistry producing •OH.[45−47] Photolysis in both chambers used two low-pressure germicidal Hg lamps (F436T5/BLC/4P-369, LCD Lighting, Inc. or GPH436T5VH/4P, Light Sources, Inc.), which were isolated from the sample flow using type 214 quartz sleeves. A fluorescent dimming ballast (IZT-2S28-D, Advance Transformer Co.) was used to regulate the current applied to the lamps. The UV irradiance was measured using a photodetector (TOCON-GaP6, sglux GmbH) and was varied by changing the control voltage applied to the ballast between 2 and 10 V. SOA particles with different O/C values were generated via gas-phase •OH oxidation of D-limonene or β-caryophyllene, followed by homogeneous nucleation. •Cl oxidation did not result in a change in O/C, even when varying lamp current and VOC injection. Across all •OH-OFR experiments, the relative humidity was controlled with a Nafion membrane humidifier (Perma Pure) to be 40 ± 10%, and the mean OFR temperature was 25 ± 4 °C. The •OH exposure in the OFR was calculated using eq 1 (adapted from Lambe et al. 2022).[44]

$$\log[OH_{exp}] = 10.098 + (0.15062 - 0.44244 \times OHR_{ext}{}^{0.1805} + 0.31146 \times \log(O_3) \times OHR_{ext}{}^{0.1672}) \times \log(O_3) + \log(H_2O) + \log\left(\frac{\tau_{OFR}}{124}\right)$$

Here, the external •OH reactivity (OHR_{ext}) is the product of the VOC concentration in cm^{-3} and its bimolecular •OH rate coefficient (cm^3 s^{-1}). Over the range of OFR185 conditions that were used for the D-limonene SOA, $•OH_{exp}$ values ranged from 2.2 × 10^{10} to 3.9 × 10^{11} cm^{-3} s, corresponding to approximately 4 h to 3 days of atmospheric oxidation at [OH] = 1.5 × 10^6 cm^{-3}.[48] For β-caryophyllene SOA studies, •OH exposure values ranged from 1.3 × 10^{11} to 2.9 × 10^{12} cm^{-3} s, corresponding to 1 to 22 days of equivalent atmospheric oxidation. Note that oxidation was dominated by •OH under the experimental conditions even though ozone was also generated in the chamber.[45]

Particle number concentrations and mobility size distributions were measured with a TSI scanning mobility particle sizer (SMPS). SOA mass concentrations were 200−700 μg m^{-3} for the D-limonene SOA and 90−1600 μg m^{-3} for the β-caryophyllene SOA. Ensemble aerosol mass spectra were measured with an Aerodyne long high-resolution time-of-flight aerosol mass spectrometer (L-ToF-AMS) or an Aerosol Chemical Speciation Monitor (ACSM), from which we calculated the fractional abundance of AMS or ACSM signals at m/z = 43 ($C_2H_3O^+$) and m/z = 44 (CO_2^+), which are used as mass spectral markers for fresh and highly aged OAs, respectively[3,16] Additionally, the oxygen-to-carbon (O/C) and hydrogen-to-carbon (H/C) ratios were obtained from L-ToF-AMS spectra using SQUIRREL/PIKA analysis software.[44] The

https://doi.org/10.1021/acsestair.5c00133
ACS EST Air 2025, 2, 1738−1749

SOA carbon oxidation state (OS_C) was calculated using the formula $OS_C = 2(O/C) - (H/C)$.[15,49] Note that this formula may slightly overestimate the carbon oxidation state, as it assumes an oxidation state of +2 for oxygen, but it should be +1 for organic peroxides. For total peroxide experiments, H/C and O/C were obtained by analyzing ACSM data using Tofware 4.0.1 (Aerodyne Research Inc.).

SOA samples were collected on PTFE filters for offline ROS and total peroxide quantification (Sections 2.2 and 2.3), high-resolution mass spectrometry analysis (Section 2.4), and photolytic aging studies (Section 2.5). Samples collected at Aerodyne were immediately stored at −4 °C until shipment under blue ice (0 °C) to UC Irvine, where they were stored in a −20 °C freezer prior to analysis. The collected SOA mass was in the range of 200−2500 μg.

2.2. Radical ROS Quantification Using Electron Paramagnetic Resonance. An X-band continuous-wave electron paramagnetic resonance (EPR) spectrometer (Bruker, Germany) was used for the quantification of radicals. All filters were analyzed with EPR within two months of sample generation. Filters were extracted in a 10 mM solution of a spin-trapping agent, 5-*tert*-butoxycarbonyl-5-methyl-1-pyrroline-*N*-oxide (BMPO, Enzo, >99%), by placing the samples on a vortex for 7 min. BMPO is efficient in trapping radicals including a hydroxyl radical ($^{\bullet}OH$), a superoxide ($O_2^{\bullet-}$)/hydroperoxyl radical ($HO_2^{\bullet}$), and carbon- and oxygen-centered organic radicals.[22,50,51] Samples were then concentrated by bubbling the solution with N_2. At 40 min, 50 μL of the sample solution was placed in a capillary tube for EPR measurements and then placed in the EPR cavity, and the sample was run at 46 min. The spectra were averaged over 10−15 scans with a center field of 3515.0 G and a sweep width of 100.0 G. The parameters for ROS measurements were as follows: an attenuation of 12 dB, a modulation amplitude of 1.0 G, a microwave power of 12.6 mW, a receiver gain of 30 dB, a microwave frequency of 9.84 GHz, and a modulation frequency of 100 kHz. Bruker SpinFit software was used to deconvolute the EPR spectra to quantify the concentrations of BMPO adducts with $^{\bullet}OH$, $O_2^{\bullet-}/HO_2^{\bullet}$, and carbon- and oxygen-centered organic radicals. The radical yield is determined by dividing the radical molar concentration determined by Bruker SpinFit software by the molar concentrations of D-limonene and β-caryophyllene SOA samples (their average molar masses were determined by HRMS).

2.3. Total Peroxide Measurements. Total peroxide (H_2O_2 and ROOH) measurements were conducted using a modified iodometric−spectrophotometric method.[25] The I_3^- absorbance of samples and standards were measured at 405 nm. The concentrations of peroxides in SOA filters were determined using a calibration curve ranging from 10 to 800 μM hydrogen peroxide solutions (Sigma-Aldrich, ≥30%). First, Milli-Q water was purged with a flow of N_2 for 30−45 min to exclude dissolved oxygen that could also slowly oxidize I^-. Using purged water, the standards, KI solution, and samples were prepared. Solid potassium iodide (KI, Sigma-Aldrich, ≥99%) was dissolved into the N_2-purged water to create a 138 μM solution. D-limonene and β-caryophyllene SOA filter samples were extracted in 1 mL of the purged water and vortexed for 7 min; 800 μL of the SOA extracts was mixed with 330 μL of glacial acetic acid (Sigma-Aldrich, ≥99%). 870 μL of the KI solution was added to the reaction vial for a final reaction volume of 2.0 mL and a final KI concentration of 60 μM, initializing the reaction. The vials were sealed immediately with parafilm and allowed to stand for 45 min. Lastly, the absorbance at 405 nm was measured using a GloMax plate reader (Promega). A blank sample filter was analyzed and fell below the limit of detection. For each VOC precursor and SOA O/C, 2−3 filter samples were analyzed, and measurements were repeated in triplicate for each SOA filter sample. The peroxide yield was determined by dividing the molarity of peroxides found in the sample solution by the molarity of the sample, with the average molar mass of the SOA compounds estimated from the HRMS analysis. Note that the measured peroxide contents should be regarded as lower limits, as water may not be able to extract all the organic peroxides in the sample, especially for the low O/C β-caryophyllene SOA,[52] and the measurements were taken more than 1 h after collection, during which highly labile peroxides may have been decomposed.[19,53]

2.4. Mass Spectrometry Analysis. We characterized the chemical composition of D-limonene and β-caryophyllene SOA samples using high-resolution mass spectrometry (HRMS) following the approach of Klodt et al. (2022)[54] and Gerritz et al. (2023).[55] SOA components were separated via ultrahigh-performance liquid chromatography (UPLC) using an HSS T3 C18 Waters Acquity Premier 150 × 2.1 mm column with 1.8 μm particles. The UPLC solvent gradient started with 95% solvent A (water acidified to pH 3 using 0.1% formic acid) and 5% solvent B (acetonitrile acidified to pH 3 using 0.1% formic acid) from 0 to 3 min. From 3 to 14 min, the solvent linearly increased to 95% B and 5% A, where it remained constant from 14 to 16 min before a linear decrease back to 95% A and 5% B from 16 to 22 min. Following UPLC, the separated mixture was detected using a Q Exactive Plus mass spectrometer (Thermo Scientific), with a resolving power of 1.4×10^5 at m/z 400. The parameters for the heated electrospray ionization (ESI) were as follows: capillary temperature, 325 °C; capillary voltage, +4.0 kV; sheath gas flow rate, 35; auxiliary gas flow rate, 10; sweep gas flow rate, 8; S-lens RF level, 30; auxiliary gas heater temperature, 300 °C. Negative ion mode data were also collected but are not included in this work.

The HRMS data were analyzed using Freestyle 1.3 (Thermo Scientific) to integrate the total ion chromatogram (TIC) from 1.3 to 14 min to generate a raw time-integrated mass spectrum. The peak positions and relative abundances were extracted by using Decon2LS software. Chromatogram features were detected using MZmine3[56] and m/z peaks containing ^{13}C, as well as sample peaks with relative abundances of less than 150% of the blank were removed using the software tools. The remaining peaks were assigned to formulas $C_cH_hO_oN_{0-2}Na_{0-1}$ (with Na only added for positive ion mode) by using an m/z accuracy of 0.001. Peaks with abnormal Kendrick mass defects were also removed, as previously described.[55] SOA O/C values for photolytic aging experiments were determined by using UPLC-HR-MS at UC Irvine. HRMS results underpredicted O/C measured by AMS, but O/C trends remained consistent across both instruments, as shown in Figure S1. The AMS O/C values are more accurate because the sensitivity of its electron impact ionization method is less compound-specific than that of the electrospray ionization method used with our UPLC-HRMS technique. All of the O/C values used in the discussion below refer to the AMS or ACSM measurements.

2.5. SOA Photolytic Aging Studies. In a subset of experiments, SOA filter samples were collected from an OFR and exposed to near-UV radiation from a xenon arc lamp

https://doi.org/10.1021/acsestair.5c00133
ACS EST Air 2025, 2, 1738−1749

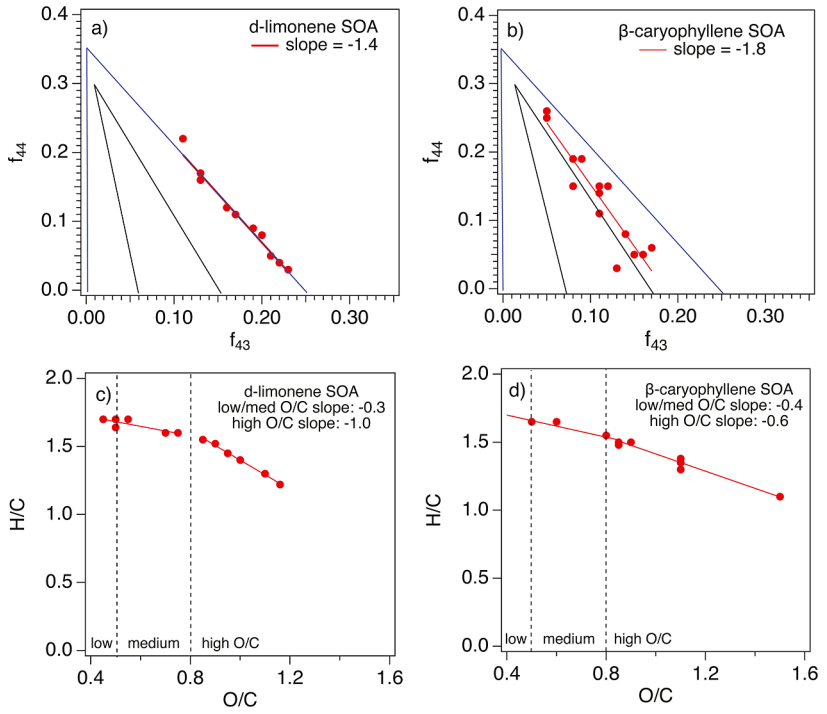

Figure 1. f_{44} vs f_{43} for (a) D-limonene SOA and (b) β-caryophyllene SOA, as measured by AMS. The inner triangular region is where most ambient samples are found,[16] and the outer triangle is where lab-generated samples are often found.[3] H/C vs O/C for (c) D-limonene SOA and (d) β-caryophyllene SOA.

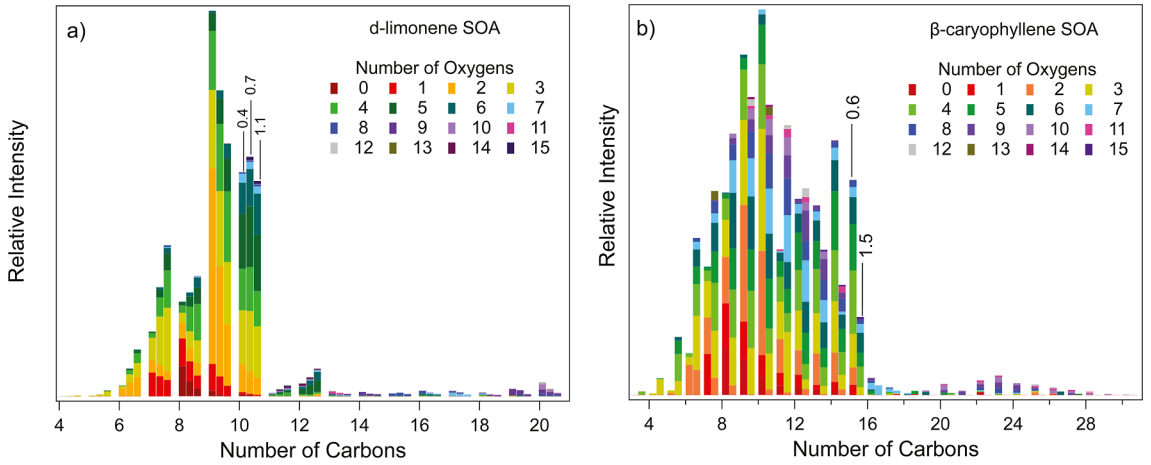

Figure 2. Carbon number with associated oxygen number of D-limonene SOA (a) and β-caryophyllene SOA (b) products. For each cluster of bars, the leftmost cluster for each carbon number is for the lowest O/C sample (O/C = 0.4 for the D-limonene SOA and O/C = 0.6 for the β-caryophyllene SOA) and the right-most cluster is for the high O/C sample (O/C = 1.1 for the D-limonene SOA and O/C = 1.5 for the β-caryophyllene SOA), as indicated by average O/C values shown for the cluster at C_{10} for the D-limonene SOA and at C_{15} for the β-caryophyllene SOA. For the D-limonene SOA, the midlevel O/C = 0.7 sample is included as the middle cluster. Relative abundance is normalized to total ion current.

(Newport model 66902).[54] The broadband light was reflected at a 90° angle with a dichroic mirror and then passed through a 295 nm long-pass filter (Schott WG295). The light was permitted to diverge so that the full filter dimension could be irradiated, but this divergence reduced the spectral flux, which is shown in Figure S2 and was measured with a spectroradiometer (PS-200, Apogee Instruments). It was estimated that 1 h of irradiation is equivalent to approximately 0.96 h under 24 h Los Angeles solar flux (taken for 20 June), as calculated for the wavelength range of 280−350 nm using the Quick TUV calculator (Madronich, 2016).[57] Photolysis was carried out for an irradiation time of 0.15−17.5 h, equivalent to 9 min to 17 h with half of a filter placed such that the filter surface was uncovered and open to laboratory air. The other half of the filter remained in the dark at room temperature for the duration of irradiation. Portions of the 18 min and 17.5 h irradiated and dark filters were analyzed using offline HRMS, as described above.

3. RESULTS

3.1. SOA Characterization with O/C and H/C. Figure 1a,b shows the plot of f_{44} vs f_{43} for D-limonene SOA and β-

https://doi.org/10.1021/acsestair.5c00133
ACS EST Air 2025, 2, 1738−1749

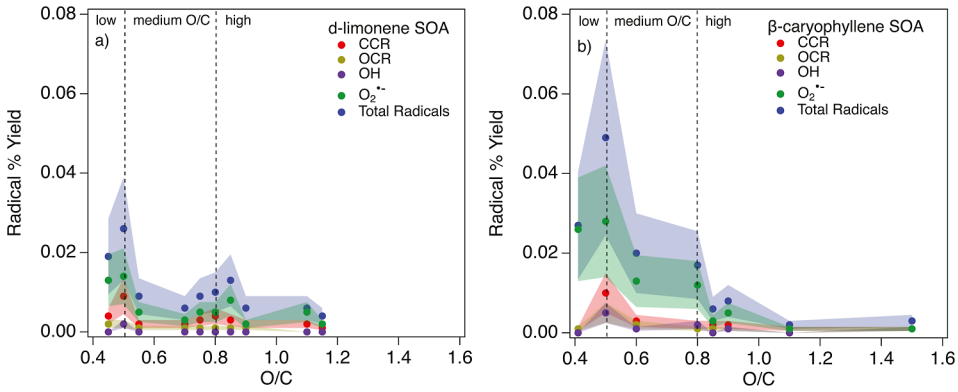

Figure 3. Radical yields in aqueous extracts of (a) D-limonene SOA and (b) β-caryophyllene SOA generated from $^{\bullet}$OH oxidation as a function of O/C. The lines represent total radicals, carbon-centered radicals (CCR), oxygen-centered organic radicals (OCR), hydroxyl radicals ($^{\bullet}$OH), and superoxide ($O_2^{\bullet-}$). Shaded regions represent error bars equaling 50% of the measured y-value including uncertainty from mass and EPR measurements.

caryophyllene SOA oxidized by OH, as measured by AMS. Two "triangle plots" are shown with inner triangles that bound ambient OA factors and an outer triangle bounding laboratory SOA.[3,58] The f_{44} values range from 0.04 to 0.22 for the D-limonene SOA and from 0.03 to 0.26 for the β-caryophyllene SOA and increase with $^{\bullet}$OH exposure.[3] The corresponding f_{43} values range from 0.11 to 0.23 (D-limonene SOA) and 0.05 to 0.17 (β-caryophyllene SOA) and decrease with $^{\bullet}$OH exposure.[3] For $^{\bullet}$Cl oxidation, f_{43} and f_{44} values remain constant regardless of $^{\bullet}$Cl or VOC concentration for both D-limonene and β-caryophyllene SOA. HRMS analysis revealed negligible differences observed in the composition of D-limonene SOA generated at different lamp intensities, as shown in Figure S3. Thus, the O/C values for D-limonene SOA and β-caryophyllene SOA generated from $^{\bullet}$Cl oxidation also remain unchanged. For $^{\bullet}$Cl oxidation, the D-limonene SOA has an O/C of 0.5 ± 0.1 and the β-caryophyllene SOA has an O/C of 0.6 ± 0.1.

Figure 1c,d shows van Krevelen diagrams that plot H/C versus O/C for D-limonene SOA and β-caryophyllene SOA, respectively, as generated via $^{\bullet}$OH oxidation. Here, O/C increases from 0.45 to 1.15 for the D-limonene SOA and from 0.40 to 1.50 for the β-caryophyllene SOA over the range of $^{\bullet}$OH exposures. In van Krevelen diagrams, the Δ(H/C)/Δ(O/C) slope provides information about oxygen-containing functional groups added to a carbon backbone.[59] A slope of 0 indicates the conversion of a C−H bond to either OH or OOH functional group; a slope of −1 indicates the conversion of a $-CH_3$ group to a C(O)OH group or installation of an OH group and a carbonyl group on two different carbon atoms; and a slope of −2 indicates the conversion of a $-CH_2-$ group to a carbonyl group.[3,28] Here, the average van Krevelen slope decreases from −0.3 (O/C = 0.45 to 0.80) to −1.0 (O/C = 0.80 to 1.15) for the D-limonene SOA and from −0.4 to −0.6 for the β-caryophyllene SOA. The differences in slopes between low and high O/C samples were found to be statistically significant (p-value <0.05) for both D-limonene SOA and β-caryophyllene SOA. Notably, this change in van Krevelen slope suggests a decrease in the yield of peroxide and/or alcohol groups in the SOA at higher $^{\bullet}$OH exposures, which is qualitatively consistent with the results presented in Section 3.4. In this work, we define ≤0.5 as low O/C, 0.5−0.8 as medium O/C, and >0.8 as high O/C.

3.2. Molecular Composition of D-Limonene and β-Caryophyllene SOA. Figure 2a shows the distribution of compounds detected in the HRMS spectra of the D-limonene SOA categorized by carbon and oxygen contents. Three sets of bars are shown that correspond to SOA samples with O/C = 0.4, 0.7, and 1.1 measured by the L-ToF-AMS. At lower carbon numbers (C_{4-8}), the O/C = 1.1 sample has a proportionally higher number of oxygens than the O/C = 0.7 and 0.4 samples. The O/C = 0.4 sample has the least number of oxygens per carbon. This is expected as high O/C or "aged" SOA should have products with higher oxygen content compared to low O/C or "fresh" SOA.[60] Following previous research, we approximately classify D-limonene SOA compounds with carbon numbers C_{4-7} as products of fragmentation, C_{8-10} as monomeric products, C_{11-15} as fragment recombination products, and C_{16-20} as dimeric products.[61,62] Dimers include C_{19-20} organic peroxides (ROOR) generated from $RO_2^{\bullet}$ + $RO_2^{\bullet}$ accretion reactions in the gas phase.[63,64] Most of the D-limonene SOA compounds have a C_n < 10, suggesting that fragmentation is a significant process over the course of multigenerational oxidative aging.[49] The O/C = 1.1 sample shows the largest abundance of fragmented products and the lowest abundance of dimers. The 0.4 °C sample, on the other hand, shows the lowest abundance of fragmented products and a higher fraction of larger carbon number species (C_{13-20+}). The higher fraction of dimers in the O/C = 0.4 sample implies a higher ROOR content. As expected, the relative intensity for the O/C = 0.7 sample falls mostly between the relative intensities for the O/C = 0.4 and O/C = 1.1 samples at all carbon numbers.

Figure 2b shows the number of oxygen atoms associated with each carbon number of the β-caryophyllene SOA products. The left-most bar for each carbon number is the low O/C sample (0.6) and the right-most bar is the high O/C sample (1.5). We observe a higher number of oxygens for carbon numbered products C_{4-16} for the high O/C sample than the low O/C sample, similar to the D-limonene SOA. Based on previous research, we consider β-caryophyllene SOA products of carbon number C_{3-13} to be fragments, C_{14-15} to be monomers, C_{16-28} to be fragment recombination products, and C_{29-30} to be dimers.[65,66] Since the majority of the β-caryophyllene SOA products have C_n < 15, this suggests that fragmentation is also significant over the course of multigenerational oxidative aging in this system. The O/C = 1.5

https://doi.org/10.1021/acsestair.5c00133
ACS EST Air 2025, 2, 1738−1749

sample shows the highest abundance of small fragments (C_{3-8}), whereas the O/C = 0.6 sample shows the largest abundance of sesquiterpene monomers (C_{14-15}), possible fragment recombination species (C_{16-28}), and dimers (C_{29-30}). We observe almost no product peaks above C_{19} for the high O/C samples, suggesting that oligomerization and higher carbon number accretion products, including peroxide dimers, are either uncommon or unstable with increasing •OH exposure. High carbon number product peaks for D-limonene and β-caryophyllene SOA are shown in Figure S4a,b.

3.3. Dependence of O/C in SOA Generation on Radical Yield. Figure 3 shows the radical yield resulting from SOA dissolution in water of D-limonene SOA (a) and β-caryophyllene SOA (b), both generated by •OH oxidation, as a function of O/C. The detected radicals include carbon-centered and oxygen-centered organic radicals (CCR and OCR), hydroxyl radicals (•OH), and superoxide ($O_2^{\bullet-}$). The D-limonene SOA with O/C = 0.45 yields 0.019 ± 0.010% ROS and the β-caryophyllene SOA with O/C = 0.41 yields 0.027 ± 0.014%. Superoxide is the primary radical observed followed by organic radicals and hydroxyl radicals. The total radical composition remains consistent across varying O/C. On average, total radicals from D-limonene SOA consist of 55% $O_2^{\bullet-}$, 31% CCR, 12% OCR, and 2% •OH. Total radicals from β-caryophyllene SOA are on average comprised of 64% $O_2^{\bullet-}$, 18% CCR, 10% OCR, and 8% •OH. Major superoxide formation from SOA agrees with a previous study by Wei et al. (2020),[22] who observed the dominant formation of superoxide and minor contribution from •OH and organic radicals by SOA samples derived from •OH oxidation of isoprene, β-pinene, α-terpineol, and D-limonene.[22]

These radicals can be generated by a cascade of aqueous-phase reactions, as initiated by the decomposition of organic hydroperoxides (ROOH) to form •OH. ROOH are generated by gas-phase multigenerational oxidation and autoxidation, as a major constituent of highly oxygenated organic molecules (HOMs) and extremely low-volatility organic compounds (ELVOCs).[24,64] The formed ROOH in the gas phase partition to the particle phase efficiently due to their low-volatility nature. In the condensed phase, ROOH are well-known to undergo thermal homolytic cleavage to generate OH radicals.[67,68] Note that •OH formation results from the decomposition of organic hydroperoxides without additional functionalities on the α-carbon, as the decomposition of α-hydroxyhydroperoxides leads to the formation of carbonyl and H_2O_2 instead of •OH.[69] The generated •OH can abstract a hydrogen atom from the α-carbon of primary or secondary alcohols to form α-hydroxyalkyl radicals, which immediately combine with dissolved O_2 to form α-hydroxyperoxyl radicals. These radicals can subsequently undergo unimolecular decomposition to form $HO_2^{\bullet}/O_2^{-\bullet}$.[22]

With an increase of O/C from 0.4 to 0.5, both D-limonene SOA and β-caryophyllene SOA exhibit an increase of ROS, including $O_2^{\bullet-}$, •OH, and organic radicals. Our observation of an initial increase in radical formation may be related to an increase in the yield of peroxide groups that generate radical ROS;[22] therefore, more radicals are expected if functionalization is occurring. Fragmentation may become more important beyond 0.5 O/C, resulting in a much less radical yield for O/C larger than 1. Figure S4a,b shows radical yield as a function of carbon oxidation state (OS_C), and similar trends are observed. These results underscore the importance of considering the O/C or OS_C when discussing ROS production by fresh and aged SOA. For SOA generated with •Cl oxidation, ROS yields were similar to that of SOA from •OH oxidation with the same O/C for D-limonene SOA (O/C = 0.5 ± 0.1) and β-caryophyllene SOA (O/C = 0.6 ± 0.1), as shown in Figure S6.

3.4. Peroxide Contents in Oxidized SOA. Figure 4 shows the measured yields of total peroxides (H_2O_2, ROOH, and ROOR) in D-limonene SOA and β-caryophyllene SOA generated with •OH oxidation. D-limonene SOA had an average peroxide yield of 19 ± 2% with an O/C of 0.30−0.40 while showing a decreased peroxide yield of 7 ± 1% with an O/C of 0.60−0.75. For β-caryophyllene SOA, the lower O/C sample (0.35−0.50 O/C) had a peroxide yield of 15 ± 5% and the high O/C sample (1.05−1.40 O/C) had a much lower yield of 2 ± 2%. The observation that samples with lower O/C are characterized by higher peroxide concentrations supports our hypothesis that the reason for higher radical generation from low O/C SOA samples is due to the higher presence of peroxides that decompose to form radical species.

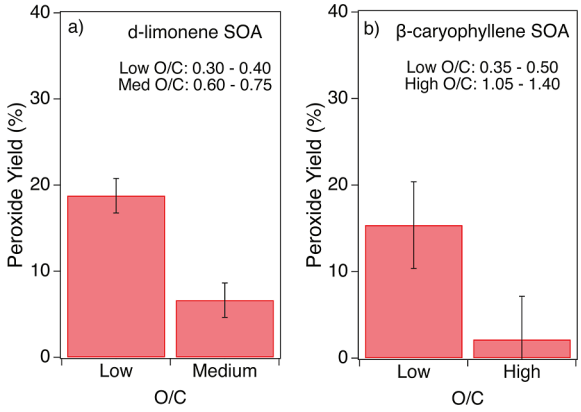

Figure 4. Peroxide yield from D-limonene SOA (a) and β-caryophyllene SOA (b) at lower and higher O/C. The error bars represent one standard deviation taken from 6 to 9 measurements.

Our results are also consistent with the labile nature of peroxides observed in other studies. A previous study by Li et al. (2022) similarly found that an anisole SOA generated less peroxides with higher •OH exposure.[33] HOMs, which contain many peroxide functional groups, were observed to be thermodynamically unstable with half-lives shorter than 1 h.[19] A photolytically aged SOA has also been found to contain reduced amounts of peroxides.[25,26,70] Spontaneous decomposition of peroxides is suggested to be an important source of ROS formation during SOA dissolution.[23,51,71−73] Our study adds to previous research by directly connecting the O/C and peroxide content, showing less peroxide contents with higher O/C.

To supplement the peroxide measurements and to investigate peroxide generation during initial SOA formation, we conducted SOA chemistry modeling with the radical 2-dimensional volatility basis set (r2D-VBS)[74−76] that considers autoxidation to evaluate the gas-phase formation of ROOH (see details in Text S1). In the model, the −OOH yield is determined based on three key reactions that depend on VOC: •OH, which are $RO_2^{\bullet} + RO_2^{\bullet}$, $RO_2^{\bullet} + HO_2^{\bullet}$, and autoxidation. The relative contribution of the three reactions depends on environmental conditions, but all three radical reactions have been observed.[77−79] Modeling results conclude that under low •OH conditions, autoxidation dominates over $RO_2^{\bullet}$ or $HO_2^{\bullet}$

https://doi.org/10.1021/acsestair.5c00133
ACS EST Air 2025, 2, 1738−1749

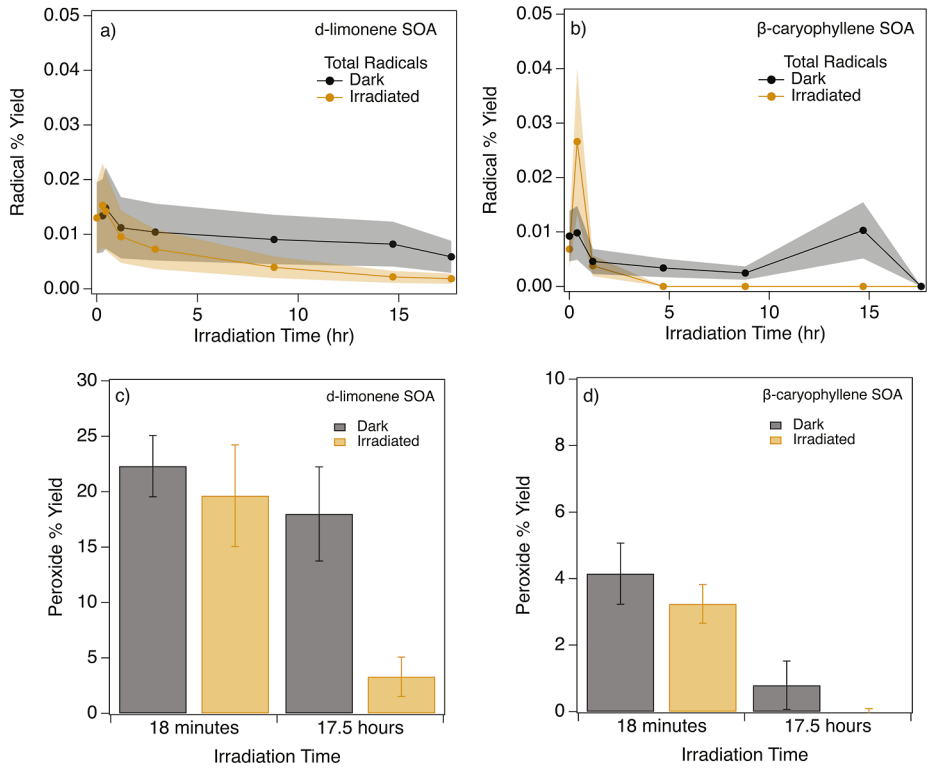

Figure 5. Radical % yield (including CCR, OCR, $^{\bullet}OH$, and $O_2^{\bullet-}$) of D-limonene SOA (a) and β-caryophyllene SOA (b) at different irradiation time points normalized to starting collection mass. Shaded regions display 50% error calculated from replicate measurements. Total peroxide yield from D-limonene SOA (c) and β-caryophyllene SOA (d) after 18 min and 17.5 h of irradiation on the filter. Error bars represent standard deviation from sample replicates.

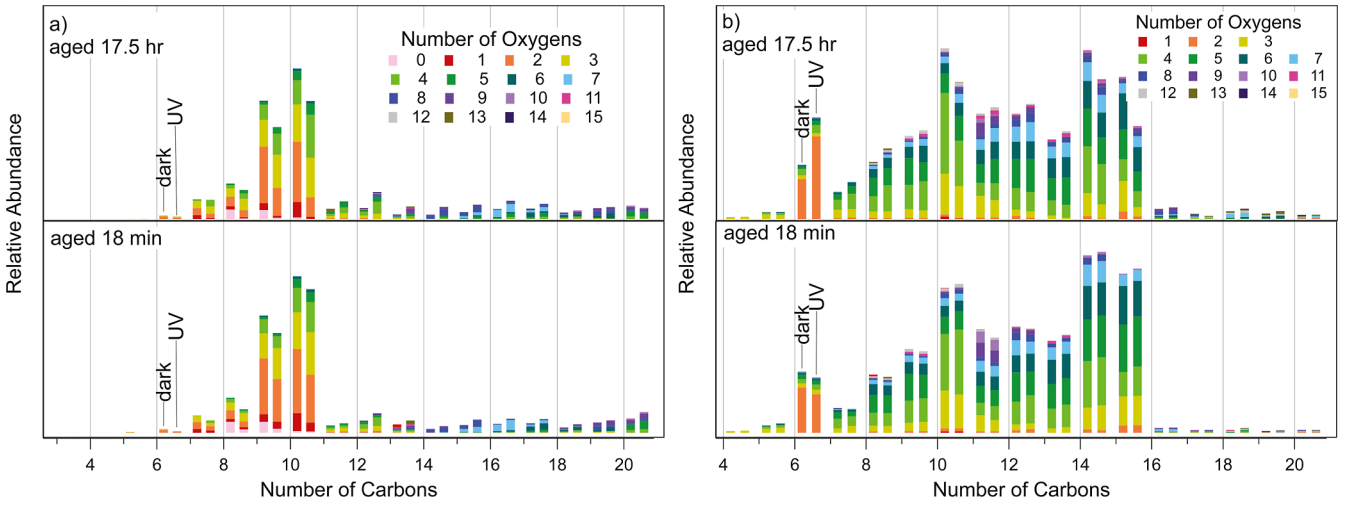

Figure 6. Relative intensity of observed compounds by carbon number (X-axis) and oxygen number (color code) in fresh (dark) and photolytically aged (UV) D-limonene SOA (a) and β-caryophyllene SOA (b) for aging times of 17.5 h and 18 min detected with HRMS in positive ion mode.

termination, generating more ROOH. Under high $^{\bullet}OH$ conditions, the $RO_2^{\bullet}$ + $RO_2^{\bullet}$ reaction dominates, resulting in a marked decrease in hydroperoxide functionality. The modeling results demonstrate that the −OOH yield decreases as $^{\bullet}OH$ exposure increases (Figure S8), as consistent with the peroxide measurements.

3.5. Effects of Photolytic Aging on ROS Formation and Peroxide Content. To provide further evidence that organic peroxides are the driving source of ROS in SOA, we conducted photolytic aging experiments on D-limonene SOA and β-caryophyllene SOA by irradiating SOA samples on filters for up to 17.5 h under lab air. Additional SOA filter samples were kept in a filter holder and wrapped in foil during the equivalent time to dark control experiments. Radical yields are normalized with the initial SOA mass. Figure 5a,b shows the total radical yield (sum of $^{\bullet}OH$, $O_2^{\bullet-}$, CCR, and OCR) from D-limonene SOA and β-caryophyllene SOA following irradiation times ranging from 18 min to 17.5 h. For both SOA, we observe an increase in radical yield after the first hour of irradiation and an hour in the dark. After 17.5 h of photoaging, the radical yield from the D-limonene SOA decreases by >80%, as shown in Figure 5a. After the β-caryophyllene SOA is aged

https://doi.org/10.1021/acsestair.5c00133
ACS EST Air 2025, 2, 1738−1749

for 5 h, we observe a similar decrease of >80% of the radical yield. Radical production for both D-limonene SOA and β-caryophyllene SOA decreases even in the dark samples, but at a slower rate than in the irradiated samples.

We measured the peroxide content of irradiated D-limonene and β-caryophyllene SOA. Peroxide yields from D-limonene and β-caryophyllene SOA irradiated for 18 min and 17.5 h are shown in Figure 5c,d. After 18 min, D-limonene SOA and β-caryophyllene SOA show a slight decrease of peroxide yield compared to their dark counterparts, but within the standard deviation. The D-limonene SOA exhibits a substantial decrease in peroxide yield from 22 ± 3% after 18 min in the dark to 3 ± 2% observed after 17.5 h of irradiation. After 17.5 h in the dark, peroxide yield also decreases slightly to 18 ± 4%. This suggests that peroxide loss by dark decomposition occurs slowly in the D-limonene SOA, but this loss is enhanced during irradiation. The β-caryophyllene SOA also shows a substantial decrease of peroxides from 4 ± 1% after 18 min in the dark to 1 ± 1% after 17.5 h of irradiation. Peroxide yield after 17.5 h in the dark also decreases substantially to 0 ± 1%, suggesting that the β-caryophyllene SOA contains more labile peroxides that may not require irradiation to decompose. After 17.5 h, peroxide content decreases substantially, which is consistent with the observed reduction of radicals observed after photoaging. Peroxides have been suggested to be significant UV absorbers in the D-limonene SOA.[80] Additionally, it has been suggested that photolabile peroxides are likely to be fragmented during irradiation,[70] and Gerritz et al. (2024) found that peroxide content in SOA was similarly diminished after irradiation.[25]

Mass spectrometry (HRMS) was applied to observe compositional changes between dark and irradiated D-limonene and β-caryophyllene SOA. Figure 6a shows the differences in the carbon and oxygen numbers between dark and irradiated samples of the D-limonene SOA after 18 min and 17.5 h of aging. After 17.5 h, we observe a decrease in the relative abundance of lower carbon numbered products, C_{3-10}, which is likely to be caused by fragmentation and evaporation of higher volatility products, and slight enhancement of C_{11-18} products, suggesting fragment recombination. There is also a slight increase in the number of oxygens associated with each carbon number after 17.5 h compared to the dark and 18 min samples, indicating further functionalization. Such oxidation may be caused by •OH generated by peroxide decomposition.[23] We observe similar trends after 18 min of aging, but the differences between the dark and irradiated are less pronounced.

After 18 min of irradiation of β-caryophyllene SOA, we observe minimal differences in both carbon number and oxygen number between the dark and irradiated samples (Figure 6b). After 17.5 h of irradiation, we observe a notable increase in C_6 species with a marginal increase in C_{4-9} and C_{11-13} products, regions associated with fragmentation products. There is some decrease in C_{10} and C_{14-15} products, for which fragmentation appears to be the dominant process, as opposed to fragment recombination for forming these species. Minor changes are observed for the higher carbon numbered species, C_{16-20}. After 17.5 h, there is a slight increase in oxygen number compared to the dark samples, which could indicate functionalization but not as significant of a change as observed with D-limonene SOA. Overall, photolytic aging has a less significant effect on SOA composition than •OH-initiated oxidative aging. However, as shown in Figure 5, photolytic aging also tends to diminish radical production because it selectively removes peroxides from SOA. As the O/C also remains mostly unchanged during irradiation for β-caryophyllene SOA (see Figure S9), this indicates that photolysis results in a different chemical process than oxidative aging.

4. IMPLICATIONS/CONCLUSIONS

This study demonstrates that upon prolonged oxidative (driven by •OH) and photolytic (driven by UV photons) aging of SOAs, labile peroxides are decomposed or fragmented, resulting in diminished spontaneous ROS production from D-limonene SOA and β-caryophyllene SOA. Free radical formation in SOA extracts was observed to be the highest at O/C = ∼0.5, followed by a decrease with an increase of O/C. Additionally, ROS generation decreased after photoirradiation for both SOA samples, even though photoirradiation induced only small changes in O/C. Our findings show •OH oxidation past an O/C > 0.5 leads to a decrease in ROS formation likely due to decomposition of peroxides, which is consistent with past studies showing functionalization of most SOA compounds until an O/C of ∼0.4, followed by fragmentation.[12,14] High-resolution mass spectrometry results show significant fragmentation of SOA compounds undergoing prolonged •OH oxidation, while such fragmentation was less significant upon extended photolytic aging. The common observation between samples with higher O/C and photoirradiated samples was a substantial reduction in peroxides, resulting in a significant decrease in the level of radical formation. While the O/C can serve as a useful metric to determine relative ROS production from SOA, peroxide contents are most critical in determining ROS formation potential by SOA.

This study suggests that the extended oxidative and photolytic aging of atmospheric biogenic SOA will reduce their ROS formation potential. Diminished ROS production may also decrease the oxidative capacity in deliquesced particles and cloud droplets, consequently altering the fates and chemical transformations of organic and inorganic chemicals in the atmosphere. Additionally, the change in ROS production has toxicological implications. Respiratory deposition of SOA particles can trigger release of ROS in the lung lining fluid.[51,71] Past studies have shown that intercellular ROS increase upon exposure to SOA with higher carbon oxidation states.[81,82] Our results suggest that low O/C SOA with higher peroxide contents would generate higher amounts of ROS compared to high O/C SOA with reduced peroxides; however, further research with cellular exposure and characterization of multiple toxicological end points is required to fully evaluate the toxicity of SOA with varied oxidation states.

■ ASSOCIATED CONTENT

Supporting Information

The Supporting Information is available free of charge at https://pubs.acs.org/doi/10.1021/acsestair.5c00133.

Comparison of O/C values determined by AMS vs HRMS; xenon Arc lamp output spectra; UPLC-HRMS results for higher carbon numbered species; radical % yield vs oxidation state of carbon for D-limonene SOA and β-caryophyllene SOA generated from •OH oxidation; radical % yield and peroxide % yield comparing •Cl and •OH oxidation for D-limonene SOA and β-caryophyllene SOA; 2D-VBS modeling results of the −OOH yield provided for D-limonene SOA over a range of •OH oxidation; and O/C shift from

https://doi.org/10.1021/acsestair.5c00133
ACS EST Air 2025, 2, 1738−1749

photolytic aging presented from UPLC-HRMS analysis (PDF)

AUTHOR INFORMATION

Corresponding Author

Manabu Shiraiwa − *Department of Chemistry, University of California, Irvine, Irvine, California 92697, United States;* orcid.org/0000-0003-2532-5373; Email: m.shiraiwa@uci.edu

Authors

Kasey C. Edwards − *Department of Chemistry, University of California, Irvine, Irvine, California 92697, United States*

Lena Gerritz − *Department of Chemistry, University of California, Irvine, Irvine, California 92697, United States;* orcid.org/0009-0009-9971-1526

Meredith Schervish − *Department of Chemistry, University of California, Irvine, Irvine, California 92697, United States;* orcid.org/0009-0002-3365-9007

Manjula Canagaratna − *Center for Aerosol and Cloud Chemistry, Aerodyne Research Inc., Billerica, Massachusetts 01821, United States*

Anita M. Avery − *Center for Aerosol and Cloud Chemistry, Aerodyne Research Inc., Billerica, Massachusetts 01821, United States;* orcid.org/0000-0002-6130-9664

Mitchell W. Alton − *Center for Aerosol and Cloud Chemistry, Aerodyne Research Inc., Billerica, Massachusetts 01821, United States;* orcid.org/0000-0002-7119-3706

Lisa M. Wingen − *Department of Chemistry, University of California, Irvine, Irvine, California 92697, United States;* orcid.org/0000-0001-5847-9913

Jackson T. Ryan − *Department of Chemistry, University of California, Irvine, Irvine, California 92697, United States;* orcid.org/0000-0002-7452-8946

Celia L. Faiola − *Department of Chemistry, University of California, Irvine, Irvine, California 92697, United States;* orcid.org/0000-0002-4987-023X

Andrew T. Lambe − *Center for Aerosol and Cloud Chemistry, Aerodyne Research Inc., Billerica, Massachusetts 01821, United States;* orcid.org/0000-0003-3031-701X

Sergey A. Nizkorodov − *Department of Chemistry, University of California, Irvine, Irvine, California 92697, United States;* orcid.org/0000-0003-0891-0052

Complete contact information is available at: https://pubs.acs.org/10.1021/acsestair.5c00133

Notes

The authors declare no competing financial interest.

ACKNOWLEDGMENTS

This work was funded by U.S. National Science Foundation through grants CHE-2203419 to UC Irvine and AGS-1934352 to Aerodyne Research Inc. The authors declare that they have no conflict of interest. We thank Madeline E. Cooke and Samuel R. La Salle for their assistance with the ACSM measurements. We thank Prof. John H. Seinfeld for inspiring younger generation through his pioneering and continuous work on secondary organic aerosols and their impacts on climate and air quality.

REFERENCES

(1) Guenther, A. B.; Jiang, X.; Heald, C. L.; Sakulyanontvittaya, T.; Duhl, T.; Emmons, L. K.; Wang, X. The Model of Emissions of Gases and Aerosols from Nature version 2.1 (MEGAN2.1): an extended and updated framework for modeling biogenic emissions. *Geosci Model Dev* **2012**, *5* (6), 1471−1492.

(2) Sakulyanontvittaya, T.; Guenther, A.; Helmig, D.; Milford, J.; Wiedinmyer, C. Secondary Organic Aerosol from Sesquiterpene and Monoterpene Emissions in the United States. *Environ. Sci. Technol.* **2008**, *42* (23), 8784−8790.

(3) Lambe, A. T.; Onasch, T. B.; Massoli, P.; Croasdale, D. R.; Wright, J. P.; Ahern, A. T.; Williams, L. R.; Worsnop, D. R.; Brune, W. H.; Davidovits, P. Laboratory studies of the chemical composition and cloud condensation nuclei (CCN) activity of secondary organic aerosol (SOA) and oxidized primary organic aerosol (OPOA). *Atmos. Chem. Phys.* **2011**, *11* (17), 8913−8928.

(4) Massoli, P.; Lambe, A. T.; Ahern, A. T.; Williams, L. R.; Ehn, M.; Mikkilä, J.; Canagaratna, M. R.; Brune, W. H.; Onasch, T. B.; Jayne, J. T.; Petäjä, T.; Kulmala, M.; Laaksonen, A.; Kolb, C. E.; Davidovits, P.; Worsnop, D. R. Relationship between aerosol oxidation level and hygroscopic properties of laboratory generated secondary organic aerosol (SOA) particles. *Geophys. Res. Lett.* **2010**, *37*, L24801.

(5) George, I. J.; Abbatt, J. P. D. Chemical evolution of secondary organic aerosol from OH-initiated heterogeneous oxidation. *Atmos. Chem. Phys.* **2010**, *10* (12), 5551−5563.

(6) Chowdhury, P. H.; He, Q.; Carmieli, R.; Li, C.; Rudich, Y.; Pardo, M. Connecting the Oxidative Potential of Secondary Organic Aerosols with Reactive Oxygen Species in Exposed Lung Cells. *Environ. Sci. Technol.* **2019**, *53* (23), 13949−13958.

(7) Offer, S.; Hartner, E.; Di Bucchianico, S.; Bisig, C.; Bauer, S.; Pantzke, J.; Zimmermann, E. J.; Cao, X.; Binder, S.; Kuhn, E.; Huber, A.; Jeong, S.; Käfer, U.; Martens, P.; Mesceriakovas, A.; Bendl, J.; Brejcha, R.; Buchholz, A.; Gat, D.; Hohaus, T.; Rastak, N.; Jakobi, G.; Kalberer, M.; Kanashova, T.; Hu, Y.; Ogris, C.; Marsico, A.; Theis, F.; Pardo, M.; Gröger, T.; Oeder, S.; Orasche, J.; Paul, A.; Ziehm, T.; Zhang, Z. H.; Adam, T.; Sippula, O.; Sklorz, M.; Schnelle-Kreis, J.; Czech, H.; Kiendler-Scharr, A.; Rudich, Y.; Zimmermann, R. Effect of Atmospheric Aging on Soot Particle Toxicity in Lung Cell Models at the Air-Liquid Interface: Differential Toxicological Impacts of Biogenic and Anthropogenic Secondary Organic Aerosols (SOAs). *Environ. Health Perspect.* **2022**, *130* (2), 027003.

(8) Lee, H. J.; Aiona, P. K.; Laskin, A.; Laskin, J.; Nizkorodov, S. A. Effect of Solar Radiation on the Optical Properties and Molecular Composition of Laboratory Proxies of Atmospheric Brown Carbon. *Environ. Sci. Technol.* **2014**, *48* (17), 10217−10226.

(9) Baboomian, V. J.; Crescenzo, G.; Huang, Y. Z.; Mahrt, F.; Shiraiwa, M.; Bertram, A. K.; Nizkorodov, S. A. Sunlight can convert atmospheric aerosols into a glassy solid state and modify their environmental impacts. *P Natl. Acad. Sci. USA* **2022**, *119* (43), No. e2208121119.

(10) Henry, K. M.; Donahue, N. M. Photochemical Aging of α-Pinene Secondary Organic Aerosol: Effects of OH Radical Sources and Photolysis. *J. Phys. Chem. A* **2012**, *116* (24), 5932−5940.

(11) Baboomian, V. J.; Gu, Y. R.; Nizkorodov, S. A. Photodegradation of Secondary Organic Aerosols by Long-Term Exposure to Solar Actinic Radiation. *ACS Earth Space Chem.* **2020**, *4* (7), 1078−1089.

(12) Kroll, J. H.; Smith, J. D.; Che, D. L.; Kessler, S. H.; Worsnop, D. R.; Wilson, K. R. Measurement of fragmentation and functionalization pathways in the heterogeneous oxidation of oxidized organic aerosol. *Phys. Chem. Chem. Phys.* **2009**, *11* (36), 8005−8014.

(13) Hall, W. A.; Pennington, M. R.; Johnston, M. V. Molecular Transformations Accompanying the Aging of Laboratory Secondary Organic Aerosol. *Environ. Sci. Technol.* **2013**, *47* (5), 2230−2237.

(14) Lambe, A. T.; Onasch, T. B.; Croasdale, D. R.; Wright, J. P.; Martin, A. T.; Franklin, J. P.; Massoli, P.; Kroll, J. H.; Canagaratna, M. R.; Brune, W. H.; Worsnop, D. R.; Davidovits, P. Transitions from Functionalization to Fragmentation Reactions of Laboratory Secon-

dary Organic Aerosol (SOA) Generated from the OH Oxidation of Alkane Precursors. *Environ. Sci. Technol.* **2012**, *46* (10), 5430−5437.
(15) Ng, N. L.; Canagaratna, M. R.; Jimenez, J. L.; Chhabra, P. S.; Seinfeld, J. H.; Worsnop, D. R. Changes in organic aerosol composition with aging inferred from aerosol mass spectra. *Atmos. Chem. Phys.* **2011**, *11* (13), 6465−6474.
(16) Ng, N. L.; Canagaratna, M. R.; Zhang, Q.; Jimenez, J. L.; Tian, J.; Ulbrich, I. M.; Kroll, J. H.; Docherty, K. S.; Chhabra, P. S.; Bahreini, R.; Murphy, S. M.; Seinfeld, J. H.; Hildebrandt, L.; Donahue, N. M.; DeCarlo, P. F.; Lanz, V. A.; Prevot, A. S. H.; Dinar, E.; Rudich, Y.; Worsnop, D. R. Organic aerosol components observed in Northern Hemispheric datasets from Aerosol Mass Spectrometry. *Atmos. Chem. Phys.* **2010**, *10* (10), 4625−4641.
(17) Mutzel, A.; Poulain, L.; Berndt, T.; Iinuma, Y.; Rodigast, M.; Böge, O.; Richters, S.; Spindler, G.; Sipilä, M.; Jokinen, T.; Kulmala, M.; Herrmann, H. Highly Oxidized Multifunctional Organic Compounds Observed in Tropospheric Particles: A Field and Laboratory Study. *Environ. Sci. Technol.* **2015**, *49* (13), 7754−7761.
(18) Ehn, M.; Thornton, J. A.; Kleist, E.; Sipilä, M.; Junninen, H.; Pullinen, I.; Springer, M.; Rubach, F.; Tillmann, R.; Lee, B.; Lopez-Hilfiker, F.; Andres, S.; Acir, I. H.; Rissanen, M.; Jokinen, T.; Schobesberger, S.; Kangasluoma, J.; Kontkanen, J.; Nieminen, T.; Kurtén, T.; Nielsen, L. B.; Jorgensen, S.; Kjaergaard, H. G.; Canagaratna, M.; Maso, M. D.; Berndt, T.; Petäjä, T.; Wahner, A.; Kerminen, V. M.; Kulmala, M.; Worsnop, D. R.; Wildt, J.; Mentel, T. F. A large source of low-volatility secondary organic aerosol. *Nature* **2014**, *506* (7489), 476−479.
(19) Krapf, M.; El Haddad, I.; Bruns, E. A.; Molteni, U.; Daellenbach, K. R.; Prévôt, A. S. H.; Baltensperger, U.; Dommen, J. Labile Peroxides in Secondary Organic Aerosol. *Chem-Us* **2016**, *1* (4), 603−616.
(20) Pöschl, U.; Shiraiwa, M. Multiphase Chemistry at the Atmosphere−Biosphere Interface Influencing Climate and Public Health in the Anthropocene. *Chem. Rev.* **2015**, *115* (10), 4440−4475.
(21) Shiraiwa, M.; Ueda, K.; Pozzer, A.; Lammel, G.; Kampf, C. J.; Fushimi, A.; Enami, S.; Arangio, A. M.; Fröhlich-Nowoisky, J.; Fujitani, Y.; Furuyama, A.; Lakey, P. S. J.; Lelieveld, J.; Lucas, K.; Morino, Y.; Pöschl, U.; Takahama, S.; Takami, A.; Tong, H.; Weber, B.; Yoshino, A.; Sato, K. Aerosol Health Effects from Molecular to Global Scales. *Environ. Sci. Technol.* **2017**, *51* (23), 13545−13567.
(22) Wei, J.; Fang, T.; Wong, C.; Lakey, P. S. J.; Nizkorodov, S. A.; Shiraiwa, M. Superoxide Formation from Aqueous Reactions of Biogenic Secondary Organic Aerosols. *Environ. Sci. Technol.* **2021**, *55* (1), 260−270.
(23) Tong, H.; Arangio, A. M.; Lakey, P. S. J.; Berkemeier, T.; Liu, F.; Kampf, C. J.; Brune, W. H.; Pöschl, U.; Shiraiwa, M. Hydroxyl radicals from secondary organic aerosol decomposition in water. *Atmos. Chem. Phys.* **2016**, *16* (3), 1761−1771.
(24) Tong, H.; Zhang, Y.; Filippi, A.; Wang, T.; Li, C.; Liu, F.; Leppla, D.; Kourtchev, I.; Wang, K.; Keskinen, H.-M.; Levula, J. T.; Arangio, A. M.; Shen, F.; Ditas, F.; Martin, S. T.; Artaxo, P.; Godoi, R. H. M.; Yamamoto, C. I.; de Souza, R. A. F.; Huang, R.-J.; Berkemeier, T.; Wang, Y.; Su, H.; Cheng, Y.; Pope, F. D.; Fu, P.; Yao, M.; Pöhlker, C.; Petäjä, T.; Kulmala, M.; Andreae, M. O.; Shiraiwa, M.; Pöschl, U.; Hoffmann, T.; Kalberer, M. Radical Formation by Fine Particulate Matter Associated with Highly Oxygenated Molecules. *Environ. Sci. Technol.* **2019**, *53* (21), 12506−12518.
(25) Gerritz, L.; Wei, J. L.; Fang, T.; Wong, C.; Klodt, A. L.; Nizkorodov, S. A.; Shiraiwa, M. Reactive Oxygen Species Formation and Peroxide and Carbonyl Decomposition in Aqueous Photolysis of Secondary Organic Aerosols. *Environ. Sci. Technol.* **2024**, *58* (10), 4716−4726.
(26) Badali, K. M.; Zhou, S.; Aljawhary, D.; Antiñolo, M.; Chen, W. J.; Lok, A.; Mungall, E.; Wong, J. P. S.; Zhao, R.; Abbatt, J. P. D. Formation of hydroxyl radicals from photolysis of secondary organic aerosol material. *Atmos. Chem. Phys.* **2015**, *15* (14), 7831−7840.
(27) Wang, S. Y.; Zhao, Y.; Chan, A. W. H.; Yao, M.; Chen, Z. M.; Abbatt, J. P. D. Organic Peroxides in Aerosol: Key Reactive Intermediates for Multiphase Processes in the Atmosphere. *Chem. Rev.* **2023**, *123* (4), 1635−1679.
(28) Chowdhury, P. H.; He, Q. F.; Male, T. L.; Brune, W. H.; Rudich, Y.; Pardo, M. Exposure of Lung Epithelial Cells to Photochemically Aged Secondary Organic Aerosol Shows Increased Toxic Effects. *Environ. Sci. Technol. Lett.* **2018**, *5* (7), 424−430.
(29) Surratt, J. D.; Murphy, S. M.; Kroll, J. H.; Ng, N. L.; Hildebrandt, L.; Sorooshian, A.; Szmigielski, R.; Vermeylen, R.; Maenhaut, W.; Claeys, M.; Flagan, R. C.; Seinfeld, J. H. Chemical composition of secondary organic aerosol formed from the photooxidation of isoprene. *J. Phys. Chem. A* **2006**, *110* (31), 9665−9690.
(30) Li, H.; Chen, Z. M.; Huang, L. B.; Huang, D. Organic peroxides' gas-particle partitioning and rapid heterogeneous decomposition on secondary organic aerosol. *Atmos. Chem. Phys.* **2016**, *16* (3), 1837−1848.
(31) Docherty, K. S.; Wu, W.; Lim, Y. B.; Ziemann, P. J. Contributions of organic peroxides to secondary aerosol formed from reactions of monoterpenes with O3. *Environ. Sci. Technol.* **2005**, *39* (11), 4049−4059.
(32) Khan, M. A. H.; Cooke, M. C.; Utembe, S. R.; Xiao, P.; Morris, W. C.; Derwent, R. G.; Archibald, A. T.; Jenkin, M. E.; Percival, C. J.; Shallcross, D. E. The global budgets of organic hydroperoxides for present and pre-industrial scenarios. *Atmos. Environ.* **2015**, *110*, 65−74.
(33) Li, C. L.; Misovich, M. V.; Pardo, M.; Fang, Z.; Laskin, A.; Chen, J. M.; Rudich, Y. Secondary organic aerosol formation from atmospheric reactions of anisole and associated health effects. *Chemosphere* **2022**, *308*, 136421.
(34) Lei, R. Y.; Wei, Z. Q.; Chen, M. J.; Meng, H. F.; Wu, Y.; Ge, X. L. Aging Effects on the Toxicity Alteration of Different Types of Organic Aerosols: A Review. *Curr. Pollut Rep* **2023**, *9* (3), 590−601.
(35) Hung, H. F.; Wang, C. S. Experimental determination of reactive oxygen species in Taipei aerosols. *J. Aerosol Sci.* **2001**, *32* (10), 1201−1211.
(36) Chen, X.; Hopke, P. K. A chamber study of secondary organic aerosol formation by linalool ozonolysis. *Atmos. Environ.* **2009**, *43* (25), 3935−3940.
(37) Wang, Y.; Kim, H.; Paulson, S. E. Hydrogen peroxide generation from α- and β-pinene and toluene secondary organic aerosols. *Atmos. Environ.* **2011**, *45* (18), 3149−3156.
(38) Zhang, Z. H.; Hartner, E.; Utinger, B.; Gfeller, B.; Paul, A.; Sklorz, M.; Czech, H.; Yang, B. X.; Su, X. Y.; Jakobi, G.; Orasche, J.; Schnelle-Kreis, J.; Jeong, S.; Gröger, T.; Pardo, M.; Hohaus, T.; Adam, T.; Kiendler-Scharr, A.; Rudich, Y.; Zimmermann, R.; Kalberer, M. Are reactive oxygen species (ROS) a suitable metric to predict toxicity of carbonaceous aerosol particles? *Atmos. Chem. Phys.* **2022**, *22* (3), 1793−1809.
(39) Coggon, M. M.; Gkatzelis, G. I.; McDonald, B. C.; Gilman, J. B.; Schwantes, R. H.; Abuhassan, N.; Aikin, K. C.; Arend, M. F.; Berkoff, T. A.; Brown, S. S.; Campos, T. L.; Dickerson, R. R.; Gronoff, G.; Hurley, J. F.; Isaacman-VanWertz, G.; Koss, A. R.; Li, M.; McKeen, S. A.; Moshary, F.; Peischl, J.; Pospisilova, V.; Ren, X.; Wilson, A.; Wu, Y.; Trainer, M.; Warneke, C. Volatile chemical product emissions enhance ozone and modulate urban chemistry. *Proc. Nat. Acad. Sci.* **2021**, *118* (32), No. e2026653118.
(40) McDonald, B. C.; de Gouw, J. A.; Gilman, J. B.; Jathar, S. H.; Akherati, A.; Cappa, C. D.; Jimenez, J. L.; Lee-Taylor, J.; Hayes, P. L.; McKeen, S. A.; Cui, Y. Y.; Kim, S.-W.; Gentner, D. R.; Isaacman-VanWertz, G.; Goldstein, A. H.; Harley, R. A.; Frost, G. J.; Roberts, J. M.; Ryerson, T. B.; Trainer, M. Volatile chemical products emerging as largest petrochemical source of urban organic emissions. *Science* **2018**, *359* (6377), 760.
(41) Gao, L.; Song, J.; Mohr, C.; Huang, W.; Vallon, M.; Jiang, F.; Leisner, T.; Saathoff, H. Kinetics, SOA yields, and chemical composition of secondary organic aerosol from β-caryophyllene ozonolysis with and without nitrogen oxides between 213 and 313 K. *Atmos. Chem. Phys.* **2022**, *22* (9), 6001−6020.
(42) Valavanidis, A.; Fiotakis, K.; Bakeas, E.; Vlahogianni, T. Electron paramagnetic resonance study of the generation of reactive

https://doi.org/10.1021/acsestair.5c00133
ACS EST Air 2025, 2, 1738−1749

oxygen species catalysed by transition metals and quinoid redox cycling by inhalable ambient particulate matter. *Redox Report* **2005**, *10* (1), 37−51.
(43) Shi, T. M.; Schins, R. P. F.; Knaapen, A. M.; Kuhlbusch, T.; Pitz, M.; Heinrich, J.; Borm, P. J. A. Hydroxyl radical generation by electron paramagnetic resonance as a new method to monitor ambient particulate matter composition. *J. Environ. Monitor* **2003**, *5* (4), 550−556.
(44) Lambe, A. T.; Avery, A. M.; Bhattacharyya, N.; Wang, D. Y.; Modi, M.; Masoud, C. G.; Ruiz, L. H.; Brune, W. H. Comparison of secondary organic aerosol generated from the oxidation of laboratory precursors by hydroxyl radicals, chlorine atoms, and bromine atoms in an oxidation flow reactor. *Environ. Sci-Atmos* **2022**, *2* (4), 687−701.
(45) Peng, Z.; Day, D. A.; Ortega, A. M.; Palm, B. B.; Hu, W.; Stark, H.; Li, R.; Tsigaridis, K.; Brune, W. H.; Jimenez, J. L. Non-OH chemistry in oxidation flow reactors for the study of atmospheric chemistry systematically examined by modeling. *Atmos. Chem. Phys.* **2016**, *16* (7), 4283−4305.
(46) Peng, Z.; Jimenez, J. L. Radical chemistry in oxidation flow reactors for atmospheric chemistry research. *Chem. Soc. Rev.* **2020**, *49* (9), 2570−2616.
(47) Rowe, J. P.; Lambe, A. T.; Brune, W. H. Technical Note: Effect of varying the λ = 185 and 254 nm photon flux ratio on radical generation in oxidation flow reactors. *Atmos. Chem. Phys.* **2020**, *20* (21), 13417−13424.
(48) Mao, J.; Ren, X.; Brune, W. H.; Olson, J. R.; Crawford, J. H.; Fried, A.; Huey, L. G.; Cohen, R. C.; Heikes, B.; Singh, H. B.; Blake, D. R.; Sachse, G. W.; Diskin, G. S.; Hall, S. R.; Shetter, R. E. Airborne measurement of OH reactivity during INTEX-B. *Atmos. Chem. Phys.* **2009**, *9* (1), 163−173.
(49) Kroll, J. H.; Donahue, N. M.; Jimenez, J. L.; Kessler, S. H.; Canagaratna, M. R.; Wilson, K. R.; Altieri, K. E.; Mazzoleni, L. R.; Wozniak, A. S.; Bluhm, H.; Mysak, E. R.; Smith, J. D.; Kolb, C. E.; Worsnop, D. R. Carbon oxidation state as a metric for describing the chemistry of atmospheric organic aerosol. *Nat. Chem.* **2011**, *3* (2), 133−139.
(50) Gerritz, L.; Schervish, M.; Lakey, P. S. J.; Oeij, T.; Wei, J.; Nizkorodov, S. A.; Shiraiwa, M. Photoenhanced Radical Formation in Aqueous Mixtures of Levoglucosan and Benzoquinone: Implications to Photochemical Aging of Biomass-Burning Organic Aerosols. *J. Phys. Chem. A* **2023**, *127* (24), 5209−5221.
(51) Wei, J.; Fang, T.; Lakey, P. S. J.; Shiraiwa, M. Iron-Facilitated Organic Radical Formation from Secondary Organic Aerosols in Surrogate Lung Fluid. *Environ. Sci. Technol.* **2022**, *56* (11), 7234−7243.
(52) Liangou, A.; Florou, K.; Psichoudaki, M.; Kostenidou, E.; Tsiligiannis, E.; Pandis, S. N. A Method for the Measurement of the Water Solubility Distribution of Atmospheric Organic Aerosols. *Environ. Sci. Technol.* **2022**, *56* (7), 3952−3959.
(53) Campbell, S. J.; Utinger, B.; Barth, A.; Leni, Z.; Zhang, Z. H.; Resch, J.; Li, K. W.; Steimer, S. S.; Banach, C.; Gfeller, B.; Wragg, F. P. H.; Westwood, J.; Wolfer, K.; Bukowiecki, N.; Ihalainen, M.; Yli-Pirilä, P.; Somero, M.; Kortelainen, M.; Louhisalmi, J.; Sklorz, M.; Czech, H.; di Bucchianico, S.; Streibel, T.; Delaval, M. N.; Ruger, C.; Baumlin, N.; Salathe, M.; Fang, Z.; Pardo, M.; D'Aronco, S.; Giorio, C.; Shi, Z. B.; Harrison, R. M.; Green, D. C.; Kelly, F. J.; Rudich, Y.; Paulson, S. E.; Sippula, O.; Zimmermann, R.; Geiser, M.; Kalberer, M. Short-lived reactive components substantially contribute to particulate matter oxidative potential. *Sci. Adv.* **2025**, *11* (12), No. eadp8100.
(54) Klodt, A. L.; Adamek, M.; Dibley, M.; Nizkorodov, S. A.; O'Brien, R. E. Effects of the sample matrix on the photobleaching and photodegradation of toluene-derived secondary organic aerosol compounds. *Atmos. Chem. Phys.* **2022**, *22* (15), 10155−10171.
(55) Gerritz, L.; Schervish, M.; Lakey, P. S. J.; Oeij, T.; Wei, J. L.; Nizkorodov, S. A.; Shiraiwa, M. Photoenhanced Radical Formation in Aqueous Mixtures of Levoglucosan and Benzoquinone: Implications to Photochemical Aging of Biomass-Burning Organic Aerosols. *J. Phys. Chem. A* **2023**, *127* (24), 5209−5221.
(56) Schmid, R.; Heuckeroth, S.; Korf, A.; Smirnov, A.; Myers, O.; Dyrlund, T. S.; Bushuiev, R.; Murray, K. J.; Hoffmann, N.; Lu, M. S.; Sarvepalli, A.; Zhang, Z.; Fleischauer, M.; Dührkop, K.; Wesner, M.; Hoogstra, S. J.; Rudt, E.; Mokshyna, O.; Brungs, C.; Ponomarov, K.; Mutabdžija, L.; Damiani, T.; Pudney, C. J.; Earll, M.; Helmer, P. O.; Fallon, T. R.; Schulze, T.; Rivas-Ubach, A.; Bilbao, A.; Richter, H.; Nothias, L. F.; Wang, M. X.; Orešič, M.; Weng, J. K.; Böcker, S.; Jeibmann, A.; Hayen, H.; Karst, U.; Dorrestein, P. C.; Petras, D.; Du, X. X.; Pluskal, T. Integrative analysis of multimodal mass spectrometry data in MZmine 3. *Nat. Biotechnol.* **2023**, *41* (4), 447−449.
(57) Madronich, S. ACOM: Quick TUV Calculator, National Center for Atmospheric Chemistry Observations and Modeling, 2016. https://www.acom.ucar.edu/Models/TUV/Interactive_TUV/(accessed 2025).
(58) Ng, N. L.; Canagaratna, M. R.; Jimenez, J. L.; Zhang, Q.; Ulbrich, I. M.; Worsnop, D. R. Real-Time Methods for Estimating Organic Component Mass Concentrations from Aerosol Mass Spectrometer Data. *Environ. Sci. Technol.* **2011**, *45* (3), 910−916.
(59) Heald, C. L.; Kroll, J. H.; Jimenez, J. L.; Docherty, K. S.; DeCarlo, P. F.; Aiken, A. C.; Chen, Q.; Martin, S. T.; Farmer, D. K.; Artaxo, P. A simplified description of the evolution of organic aerosol composition in the atmosphere. *Geophys. Res. Lett.* **2010**, *37*, L08803.
(60) Ayres, J. G.; Borm, P.; Cassee, F. R.; Castranova, V.; Donaldson, K.; Ghio, A.; Harrison, R. M.; Hider, R.; Kelly, F.; Kooter, I. M.; Marano, F.; Maynard, R. L.; Mudway, I.; Nel, A.; Sioutas, C.; Smith, S.; Baeza-Squiban, A.; Cho, A.; Duggan, S.; Froines, J. Evaluating the Toxicity of Airborne Particulate Matter and Nanoparticles by Measuring Oxidative Stress Potential—A Workshop Report and Consensus Statement. *Inhalation Toxicol.* **2008**, *20* (1), 75−99.
(61) Liu, D. D.; Zhang, Y.; Zhong, S. J.; Chen, S.; Xie, Q. R.; Zhang, D. H.; Zhang, Q.; Hu, W.; Deng, J. J.; Wu, L. B.; Ma, C.; Tong, H. J.; Fu, P. Q. Large differences of highly oxygenated organic molecules (HOMs) and low-volatile species in secondary organic aerosols (SOAs) formed from ozonolysis of β-pinene and limonene. *Atmos. Chem. Phys.* **2023**, *23* (14), 8383−8402.
(62) Molteni, U.; Simon, M.; Heinritzi, M.; Hoyle, C. R.; Bernhammer, A. K.; Bianchi, F.; Breitenlechner, M.; Brilke, S.; Dias, A.; Duplissy, J.; Frege, C.; Gordon, H.; Heyn, C.; Jokinen, T.; Kürten, A.; Lehtipalo, K.; Makhmutov, V.; Petäjä, T.; Pieber, S. M.; Praplan, A. P.; Schobesberger, S.; Steiner, G.; Stozhkov, Y.; Tomé, A.; Tröstl, J.; Wagner, A. C.; Wagner, R.; Williamson, C.; Yan, C.; Baltensperger, U.; Curtius, J.; Donahue, N. M.; Hansel, A.; Kirkby, J.; Kulmala, M.; Worsnop, D. R.; Dommen, J. Formation of Highly Oxygenated Organic Molecules from α-Pinene Ozonolysis: Chemical Characteristics, Mechanism, and Kinetic Model Development. *ACS Earth Space Chem.* **2019**, *3* (5), 873−883.
(63) Peräkylä, O.; Berndt, T.; Franzon, L.; Hasan, G.; Meder, M.; Valiev, R. R.; Daub, C. D.; Varelas, J. G.; Geiger, F. M.; Thomson, R. J.; Rissanen, M.; Kurtén, T.; Ehn, M. Large Gas-Phase Source of Esters and Other Accretion Products in the Atmosphere. *J. Am. Chem. Soc.* **2023**, *145* (14), 7780−7790.
(64) Bianchi, F.; Kurtén, T.; Riva, M.; Mohr, C.; Rissanen, M. P.; Roldin, P.; Berndt, T.; Crounse, J. D.; Wennberg, P. O.; Mentel, T. F.; Wildt, J.; Junninen, H.; Jokinen, T.; Kulmala, M.; Worsnop, D. R.; Thornton, J. A.; Donahue, N.; Kjaergaard, H. G.; Ehn, M. Highly Oxygenated Organic Molecules (HOM) from Gas-Phase Autoxidation Involving Peroxy Radicals: A Key Contributor to Atmospheric Aerosol. *Chem. Rev.* **2019**, *119* (6), 3472−3509.
(65) Jokinen, T.; Kausiala, O.; Garmash, O.; Peräkylä, O.; Junninen, H.; Schobesberger, S.; Yan, C.; Sipilä, M.; Rissanen, M. P. Production of highly oxidized organic compounds from ozonolysis of β-caryophyllene : laboratory and field measurements. *Boreal Environment Research* **2016**, *21* (3−4), 262−273.
(66) Gao, L. Y.; Song, J. W.; Mohr, C.; Huang, W.; Vallon, M.; Jiang, F.; Leisner, T.; Saathoff, H. Kinetics, SOA yields, and chemical composition of seconaary organic aerosol from β-caryophyllene

https://doi.org/10.1021/acsestair.5c00133
ACS EST Air 2025, 2, 1738−1749

ozonolysis with and without nitrogen oxides between 213 and 313 K. *Atmos. Chem. Phys.* **2022**, *22* (9), 6001−6020.
(67) Nam, W.; Han, H. J.; Oh, S.-Y.; Lee, Y. J.; Choi, M.-H.; Han, S.-Y.; Kim, C.; Woo, S. K.; Shin, W. New Insights into the Mechanisms of O−O Bond Cleavage of Hydrogen Peroxide and tert-Alkyl Hydroperoxides by Iron(III) Porphyrin Complexes. *J. Am. Chem. Soc.* **2000**, *122* (36), 8677−8684.
(68) Tong, H.; Arangio, A. M.; Lakey, P. S. J.; Berkemeier, T.; Liu, F.; Kampf, C. J.; Brune, W. H.; Pöschl, U.; Shiraiwa, M. Hydroxyl radicals from secondary organic aerosol decomposition in water. *Atmos. Chem. Phys.* **2016**, *16*, 1761−1771.
(69) Qiu, J.; Liang, Z.; Tonokura, K.; Colussi, A. J.; Enami, S. Stability of Monoterpene-Derived α-Hydroxyalkyl-Hydroperoxides in Aqueous Organic Media: Relevance to the Fate of Hydroperoxides in Aerosol Particle Phases. *Environ. Sci. Technol.* **2020**, *54* (7), 3890−3899.
(70) Epstein, S. A.; Blair, S. L.; Nizkorodov, S. A. Direct Photolysis of a-Pinene Ozonolysis Secondary Organic Aerosol: Effect on Particle Mass and Peroxide Content. *Environ. Sci. Technol.* **2014**, *48* (19), 11251−11258.
(71) Tong, H.; Lakey, P. S. J.; Arangio, A. M.; Socorro, J.; Shen, F. X.; Lucas, K.; Brune, W. H.; Pöschl, U.; Shiraiwa, M. Reactive Oxygen Species Formed by Secondary Organic Aerosols in Water and Surrogate Lung Fluid. *Environ. Sci. Technol.* **2018**, *52* (20), 11642−11651.
(72) Tong, H.; Lakey, P. S. J.; Arangio, A. M.; Socorro, J.; Kampf, C. J.; Berkemeier, T.; Brune, W. H.; Pöschl, U.; Shiraiwa, M. Reactive oxygen species formed in aqueous mixtures of secondary organic aerosols and mineral dust influencing cloud chemistry and public health in the Anthropocene. *Faraday Discuss.* **2017**, *200* (0), 251−270.
(73) Tong, H. J.; Liu, F. B.; Filippi, A.; Wilson, J.; Arangio, A. M.; Zhang, Y.; Yue, S. Y.; Lelieveld, S.; Shen, F. X.; Keskinen, H. M. K.; Li, J.; Chen, H. X.; Zhang, T.; Hoffmann, T.; Fu, P. Q.; Brune, W. H.; Petäjä, T.; Kulmala, M.; Yao, M. S.; Berkemeier, T.; Shiraiwa, M.; Pöschl, U. Aqueous-phase reactive species formed by fine particulate matter from remote forests and polluted urban air. *Atmos. Chem. Phys.* **2021**, *21* (13), 10439−10455.
(74) Schervish, M.; Donahue, N. M. Peroxy radical chemistry and the volatility basis set. *Atmos. Chem. Phys.* **2020**, *20* (2), 1183−1199.
(75) Schervish, M.; Heinritzi, M.; Stolzenburg, D.; Dada, L.; Wang, M. Y.; Ye, Q.; Hofbauer, V.; Devivo, J.; Bianchi, F.; Brilke, S.; Duplissy, J.; El Haddad, I.; Finkenzeller, H.; He, X. C.; Kvashnin, A.; Kim, C.; Kirkby, J.; Kulmala, M.; Lehtipalo, K.; Lopez, B.; Makhmutov, V.; Mentler, B.; Molteni, U.; Nie, W.; Petäjä, T.; Quéléver, L.; Volkamer, R.; Wagner, A. C.; Winkler, P.; Yan, C.; Donahue, N. M. Interactions of peroxy radicals from monoterpene and isoprene oxidation simulated in the radical volatility basis set. *Environ. Sci-Atmos* **2024**, *4* (7), 740−753.
(76) Schervish, M.; Donahue, N. M. Peroxy radical kinetics and new particle formation. *Enviiron. Sci. Atmos.* **2021**, *1* (2), 79−92.
(77) Mohr, C.; Lopez-Hilfiker, F. D.; Yli-Juuti, T.; Heitto, A.; Lutz, A.; Hallquist, M.; D'Ambro, E. L.; Rissanen, M. P.; Hao, L. Q.; Schobesberger, S.; Kulmala, M.; Mauldin, R. L.; Makkonen, U.; Sipilä, M.; Petäjä, T.; Thornton, J. A. Ambient observations of dimers from terpene oxidation in the gas phase: Implications for new particle formation and growth. *Geophys. Res. Lett.* **2017**, *44* (6), 2958−2966.
(78) Orlando, J. J.; Tyndall, G. S. Laboratory studies of organic peroxy radical chemistry: an overview with emphasis on recent issues of atmospheric significance. *Chem. Soc. Rev.* **2012**, *41* (24), 6294.
(79) Zhao, Y.; Thornton, J. A.; Pye, H. O. T. Quantitative constraints on autoxidation and dimer formation from direct probing of monoterpene-derived peroxy radical chemistry. *P Natl. Acad. Sci. USA* **2018**, *115* (48), 12142−12147.
(80) Walser, M. L.; Park, J.; Gomez, A. L.; Russell, A. R.; Nizkorodov, S. A. Photochemical aging of secondary organic aerosol particles generated from the oxidation of d-limonene. *J. Phys. Chem. A* **2007**, *111* (10), 1907−1913.
(81) Tuet, W. Y.; Chen, Y.; Fok, S.; Champion, J. A.; Ng, N. L. Inflammatory responses to secondary organic aerosols (SOA) generated from biogenic and anthropogenic precursors. *Atmos. Chem. Phys.* **2017**, *17* (18), 11423−11440.
(82) Tuet, W. Y.; Chen, Y.; Fok, S.; Gao, D.; Weber, R. J.; Champion, J. A.; Ng, N. L. Chemical and cellular oxidant production induced by naphthalene secondary organic aerosol (SOA): effect of redox-active metals and photochemical aging. *Sci. Rep.* **2017**, *7* (1), 15157.

https://doi.org/10.1021/acsestair.5c00133
ACS EST Air 2025, 2, 1738−1749